Journal of Solid State Chemistry **148,** 361–369 (1999)
Article ID jssc.1999.8461, available online at http://www.idealibrary.com on IDEAL®

Structural and Magnetic Characterization of $NdCaCrO_4$ Oxide

J. Romero de Paz,* J. Hernández Velasco,* M. T. Fernández-Díaz,† P. Porcher,‡ J. L. Martínez,§ and R. Sáez Puche*,[1]

** Departamento de Química Inorgánica, Facultad Ciencias Químicas. Universidad Complutense de Madrid, E-2840 Madrid, Spain; †Institut Laue-Langevin, BP 156X, F-38042 Grenoble Cedex, France; ‡Laboratoire de Chimie Appliquée de l'Etat Solide, CNRS-UMR 7574, 11 rue P. et M. Curie, F-75231 CX05 Paris, France; and §Instituto de Ciencia de Materiales de Madrid, CSIC, Cantoblanco, E-28049 Madrid, Spain*

Received March 16, 1999; in revised form June 24, 1999; accepted July 22, 1999

The structural and magnetic properties of $NdCaCrO_4$ oxide have been studied mainly by means of neutron powder diffraction. This oxide presents orthorhombic symmetry, space group *Bmab*, with lattice parameters at room temperature $a = 5.3739(1)$ Å, $b = 5.54114(1)$ Å, and $c = 11.9536(3)$ Å. At around 973 K a reversible phase transition to a tetragonal (*I*4/*mmm*) structure has been determined from X-ray powder diffraction data. Below 180 K, $NdCaCrO_4$ shows antiferromagnetic ordering in the Cr^{3+} sublattice that has been explained on the basis of a propagation vector k = 0 and a collinear magnetic structure, with a symmetry mode G_x. At 30 K an antiferromagnetic ordered component along the *z* direction appears. This spin reorientation could be induced by the onset of local magnetic interactions between the neodymium and chromium sublattices.

Key Words: **$NdCaCrO_4$ oxide; antiferromagnetic order; magnetic structure; spin reorientation.**

1. INTRODUCTION

Many compounds with the K_2NiF_4-type structure (1) have been intensively investigated starting from the discovery of the high temperature superconductivity in the $La_{1.85}Ba_{0.15}CuO_4$ oxide (2). Among them, as possible candidates to show the superconductivity phenomenon, are the R_2NiO_4 oxides where *R* is the La^{3+}, Pr^{3+}, and Nd^{3+} ions. The structure of these oxides presents orthorhombic symmetry, space group *Bmab*, at room temperature (RT). It has been determined that this orthorhombic distortion from the ideal K_2NiF_4-type is owing to a coupled tilt of the (NiO_6) octahedra present in the structure (3) that takes place with the aim of diminishing the two-dimensional lattice mismatch between the two layers that are intergrown: the double NaCl-type $(RO)_2$ layer and the square (NiO_2) layer (4). This orthorhombic strain increases with the decreasing size of the rare earth ion (5). This feature of structural mismatch is a steric characteristic of this structural type, but will depend strongly on the relation between the 3*d* metal and the rare earth ionic sizes. Thus, it will be important to compare the different behaviors depending on the 3*d* metal and the rare earth ions. Most of the data available in the literature are related to Ni and Cu compounds but very little information is known for different 3*d* metals such as Cr.

Neutron diffraction studies on stoichiometric R_2NiO_4 oxides have determined the existence of two different structural phase transitions (3, 6–9) at low and high temperature. The low temperature phase has a tetragonal average structure, space group $P4_2/ncm$, and the high temperature phase has a tetragonal structure too, but space group $I4/mmm$. From a magnetic point of view, in the three compounds Ni^{2+} ions order antiferromagnetically at about 325 K and at low temperatures the Nd^{3+} or Pr^{3+} ions are also involved in the magnetic order (5, 6, 8–10).

Within this framework we have tackled the study of the $RCaCrO_4$ oxides (*R*, rare earth). These oxides, with *R* as Pr, Nd, Sm, Eu, and Gd, were prepared by Daoudi and Le Flem (11) and partly characterized by means of X-ray diffraction. However, further studies concerning the structural and magnetic characterization show clearly the presence of $RCrO_3$ perovskite as an impurity (12–14), with a strong ferromagnetic behavior which makes impossible the magnetic characterization of the $RCaCrO_4$ oxides.

Bearing all this in mind, in this work we present the specific conditions in the preparation of the $NdCaCrO_4$ oxide as pure phase and the detailed structural and magnetic characterization, by means of X-ray and neutron powder diffraction. It is worth noting that in a previous work we have studied the isostructural $PrCaCrO_4$ oxide (15) and so, we present a comparative study between both isostructural oxides. An explanation of the different magnetic behavior observed at low temperature is justified from the crystal field ground term of the rare earth trivalent ion.

[1] To whom correspondence should be addressed.

0022-4596/99 $30.00

2. EXPERIMENTAL DETAILS

The polycrystalline brown $NdCaCrO_4$ oxide was prepared by solid state reaction of the stoichiometric amounts of the high purity oxides Nd_2O_3 and Cr_2O_3, and a 20 wt% excess of $CaCO_3$ (AR grade) to avoid the presence of $NdCrO_3$ as an impurity. The homogenized mixture was heated under argon flow at 1360°C for 26 hours; then the sample was ground and reheated in argon at 1370°C for 18 hours. The X-ray diffraction pattern of this sample shows the existence of $NdCaCrO_4$, CaO (~4%), and Nd_2O_3 (~2%) phases, the latter owing to the Cr_2O_3 volatility. In order to check the presence of interstitial oxygen, giving rise to the nonstoichiometric $NdCaCrO_{4+\delta}$ samples, we carried out TGA measurements in a Cahn D-2000 electrobalance under reducing atmosphere He-(5%)H_2. The obtained result shows that the sample can be formulated as $NdCaCrO_4$ ($\delta \approx 0$).

X-ray powder diffraction patterns at RT were recorded using a Philips X' Pert MPD diffractometer, while X-ray powder diffraction patterns at high temperature were obtained using a Siemens D-5000 diffractometer with an Anton Paar KG HTK10 high temperature camera. Both diffractometers work with $\lambda_{Cu} = 1.5418$ Å. The neutron powder diffraction experiments were carried out in the High Flux Reactor at the Institute Laue Langevin (Grenoble, France). Two different diffractometers were used: the medium resolution D1B ($\lambda = 2.5251$ Å), to study the thermal evolution of the sample in a temperature range between 1.5 and 250 K, and the high resolution D2B ($\lambda = 1.594$ Å), to get an accurate structural characterization at RT (16). All the powder diffraction data were analyzed with the Rietveld method (17), using the FULLPROF program (18). A pseudo-Voigt profile function without preferred crystallite orientation was used.

Magnetization measurements were performed in a Quantum Design XL-SQUID magnetometer, between 1.7 and 300 K. The magnetization data versus temperature were obtained in a zero field cooling method with an applied magnetic field of 500 Oe. The magnetic susceptibility measurements from 300 to 600 K were performed with a DSM8 magnetosusceptometer in helium atmosphere to avoid the sample decomposition that takes place in this temperature range when the $NdCaCrO_4$ is heated in air.

3. RESULTS AND DISCUSSION

3.1. Structural Characterization

The $NdCaCrO_4$ oxide presents at RT orthorhombic symmetry, space group *Bmab*. Figure 1 shows the high resolution neutron diffraction pattern obtained at RT for $NdCaCrO_4$, refined on the basis of the *Bmab* space group, with Nd^{3+} and Ca^{2+} ions randomly distributed in the same Wyckoff position. The structural parameters obtained from the Rietveld refinement are shown in Table 1. The orthorhombic distortion can be evaluated through the orthorhombic strain parameter S_o, defined as $2(b-a)/(b+a)$, and it has been observed that the $NdCaCrO_4$ compound ($S_o = 6.95(4) \times 10^{-3}$) presents a larger orthorhombic distortion than the $PrCaCrO_4$ oxide ($S_o = 4.04(7) \times 10^{-3}$). This is due to the smaller size of the Nd^{3+} ion. The (CrO_6) octahedra are tilted having the [100] direction as tilt axis, clockwise and counterclockwise alternately along the [010] direction. This tilting can be quantified through the α_1 and α_2 angles, in such a way that α_1 is formed by the equatorial plane of the octahedron and the basal plane xy of the unit cell, and α_2 is defined by the Cr–O axial bond of the octahedron and the z-axis of the unit cell. These angles are slightly different at RT, α_1 being smaller than α_2 (see Table 1), whereas in the case of the isomorphous $PrCaCrO_4$ oxide they are almost identical with a value of 4.0(1)°. Both angles obtained in the case of the $NdCaCrO_4$ oxide are greater than those found in $PrCaCrO_4$, according to the larger orthorhombic distortion of the neodymium phase. The meodymium and calcium atoms are nine-fold coordinated and the coordination polyhedron is a monocapped square antiprism; see Fig. 2. This coordination polyhedron is strongly distorted with six different distances (see Table 1): there are two distances to four oxygen atoms (*a* and *b*) which belong to the nearest-neighbor CrO_2 layer, three distances to four oxygen atoms (*d*, *e*, and *f*) which belong to the same $Nd_{1/2}Ca_{1/2}O$ layer, and the shortest one to the apical oxygen atom (*c*) which belongs to the nearest-neighbor $Nd_{1/2}Ca_{1/2}O$ layer. This distortion, as can be clearly observed, is due to the mentioned tilt of the (CrO_6) octahedra. The (CrO_6) octahedra are tetragonally distorted with a $d_{Cr-Oaxial}/d_{Cr-Oequatorial}$ ratio of 1.06; see Table 1. Moreover, as a consequence of the orthorhombic distortion, the γO–Cr–O angle within the octahedra basal plane takes the value of 89.6(1)°; see Fig. 2.

Figure 3 shows the thermal dependence of the lattice parameters *a* and *b* obtained from X-ray diffraction at high temperature. A gradual increase of the *a* parameter with the temperature can be observed, whereas the *b* parameter shows a slight decrease. Both parameters become coincident at 973 K, indicative of the existence of a reversible phase transition of the type Orthorhombic (*Bmab*) → Tetragonal (*I*4/*mmm*), which is similar to that found in the isostructural La_2NiO_4 oxide (6). The continuous variation of the order parameter points to a phase transition of the second order. The lattice parameter plotted in the tetragonal phase region of Fig. 3 is $\sqrt{2}a_{T_t}$, where a_{T_t} corresponds to the lattice parameter of the tetragonal body centered unit cell.

The structural characterization of the $NdCaCrO_4$ oxide below RT has been made by neutron powder diffraction measurements. Figure 4 shows the temperature variation of

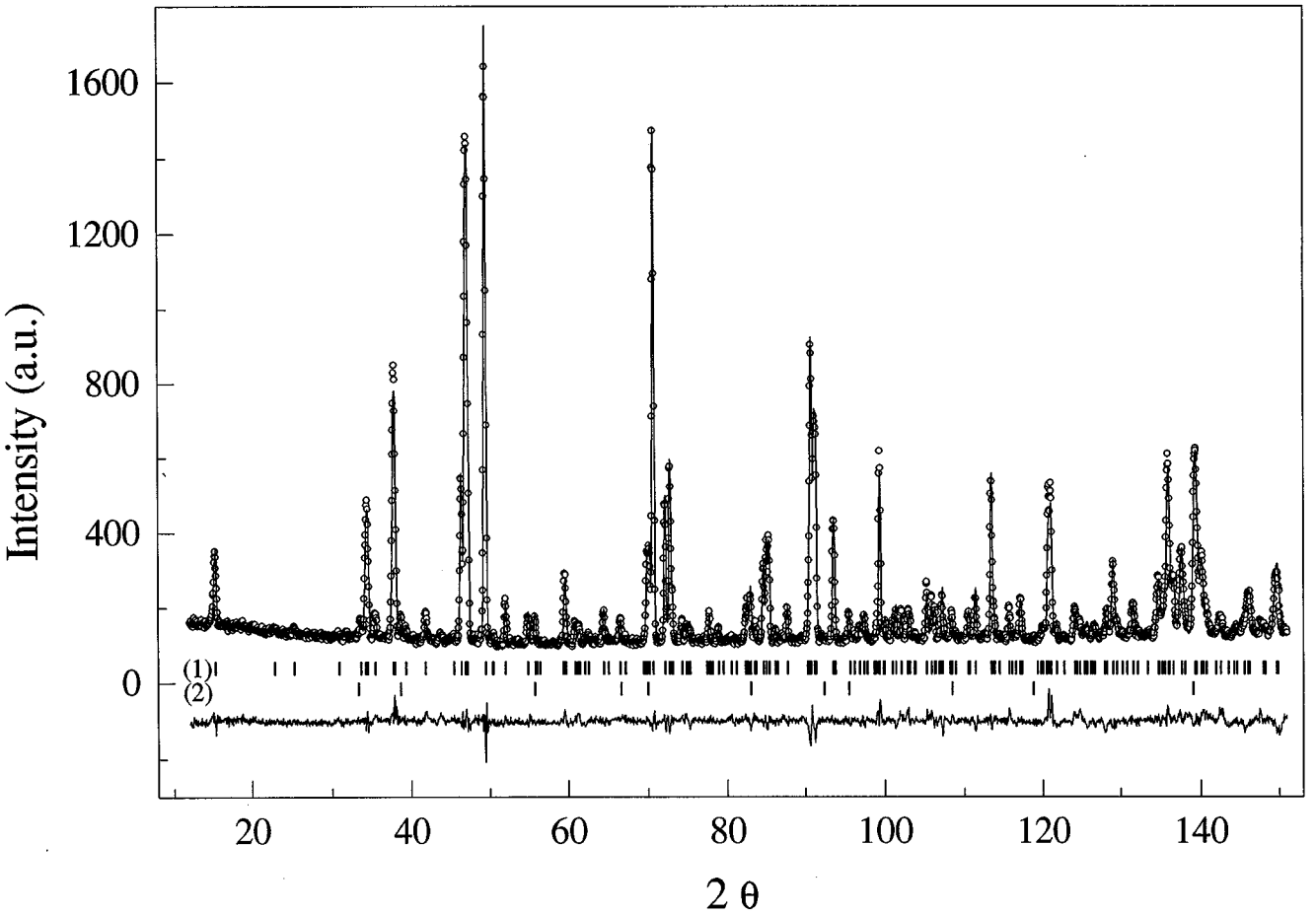

FIG. 1. High resolution neutron powder diffraction pattern obtained at 300 K (circles) and calculated (solid line) for $NdCaCrO_4$ oxide. Vertical marks show the position of allowed structural Bragg reflections for $NdCaCrO_4$ (1) and CaO (2) oxides. A difference curve is plotted at the bottom of the pattern. Reliability factors: $R_{wp} = 12.6$ %, $R_B = 6.66\%$, and $\chi^2 = 2.63$.

the diffraction patterns in the 2θ angular range 53 to 59 degrees, between 250 and 10 K. The merging of the reflections (200) and (020) upon cooling with an apparent intensity increase up to 150 K due to the narrowing can be observed. Below this temperature the intensity remains almost constant. This shows a tendency in the system toward tetragonality. Nevertheless, the powder diffraction data have been refined on the basis of an orthorhombic symmetry, space group *Bmab*. In Fig. 5 the thermal evolution of the lattice parameters *a* and *b* from 250 to 1.5 K is shown. On decreasing the temperature, both parameters remain practically constant until the temperature reaches the value of 180 K. At this temperature *a* and *b* parameters undergo a sudden increase and decrease, respectively. Below 100 K they remain almost constant down to 1.5 K. In La_2NiO_4 oxide a similar but more pronounced variation in the lattice parameters has been found (3). It has been associated with a first order phase transition of the type orthorhombic (*Bmab*) to Tetragonal ($P4_2/ncm$) symmetry. However, the Rietveld refinements of the powder diffraction patterns obtained at low temperature for the $NdCaCrO_4$ oxide on the basis of a tetragonal symmetry, space group $P4_2/ncm$, do not give rise to a better result than considering orthorhombic symmetry, space group *Bmab*. Therefore, the existence of such a phase transition in the $NdCaCrO_4$ oxide cannot be determined certainly, it being necessary to obtain single crystal diffraction data to clarify this point. From all this, we will consider that the orthorhombic symmetry, space group *Bmab*, remains until 1.5 K.

3.2. Magnetic Behavior

Despite the lack of explicit calculation of the ratio between interplane and intraplane *J* exchange constants, a more pronounced 3D magnetic behavior is expected for $RCaCrO_4$ compared with R_2NiO_4 and R_2CuO_4, whose 2D behavior is favored by larger *M*–O(2) distances, taking into account that the pathway for interplane superexchange interactions proceeds through the apical oxygen of the MO_6 octahedra.

TABLE 1
Structural Parameters of $NdCaCrO_4$ Oxide at RT Obtained from Rietveld Refinement of High Resolution Neutron Powder Diffraction Data

$a = 5.3739(1)$ Å		Site	x	y	z
$b = 5.4114(1)$ Å					
$c = 11.9536(3)$ Å	Nd/Ca	8*f*	0	− 0.0081(7)	0.3585(2)
$V = 347.615(9)$ Å^3	Cr	4*a*	0	0	0
$B_{overall} = 0.65(3)$ Å^2	O1	8*e*	1/4	1/4	− 0.0093(3)
	O2	8*f*	0	0.0341(6)	0.1692(3)

Cr–O1 (×4) = 1.9114(3) Å	Nd/Ca–O1 (×2) = 2.501(3) Å	(a)
Cr–O2 (×2) = 2.039(3) Å	Nd/Ca–O1 (×2) = 2.602(3) Å	(b)
	Nd/Ca–O2 (×1) = 2.274(4) Å	(c)
$\alpha_1 = 4.7(1)^\circ$	Nd/Ca–O2 (×1) = 2.499(6) Å	(d)
$\alpha_2 = 5.2(1)^\circ$	Nd/Ca–O2 (×1) = 2.953(6) Å	(e)
	Nd/Ca–O2 (×2) = 2.7109(5) Å	(f)

Note. Numbers in parentheses are estimated standard deviations.

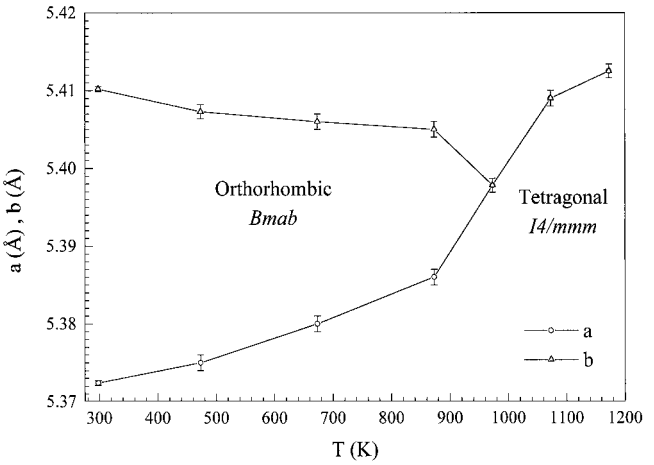

FIG. 3. Temperature dependence of the lattice parameters *a* and *b* above RT for $NdCaCrO_4$ oxide obtained from X-ray powder diffraction. The lines are drawn to guide the eye.

Figure 6 shows the temperature dependence of the magnetic susceptibility between 1.7 and 600 K. In the 300 to 600 K temperature range the magnetic susceptibility obeys a Curie–Weiss law, $\chi = 3.60/(T + 241.2)$, and the calculated magnetic moment is $5.38\,\mu_B$, which is slightly higher than expected for the paramagnetic contribution of Nd^{3+} and Cr^{3+} ions. Below 300 K the thermal evolution of the reciprocal magnetic susceptibility, see inset in Fig. 6, shows the existence of a very tenuous inflection point around 170 K that could be due to the onset of antiferromagnetic ordering in the Cr^{3+} sublattice, like in the case of $PrCaCrO_4$ oxide (15). These antiferromagnetic interactions have been confirmed by neutron diffraction data, as will be discussed later. The downward deviations from the Curie–Weiss behavior observed below 150 K can be assigned to the characteristic behavior of the Nd^{3+} ground state ($^4I_{9/2}$) under the influence of the crystal field. However, at very low temperature there is a gradual loss of the magnetic susceptibility signal.

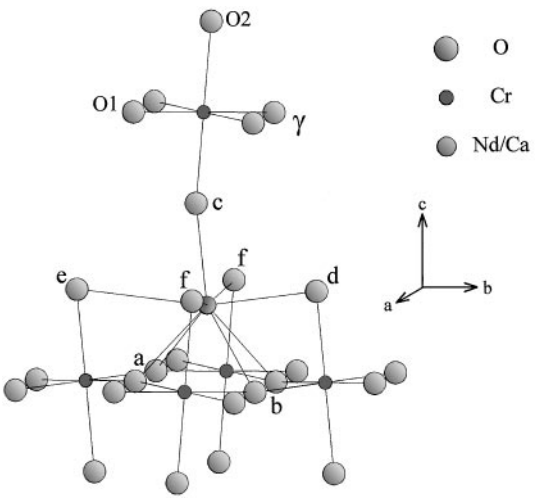

FIG. 2. Chemical environment of Nd/Ca and Cr atoms. The Arabic letters point out the six different Nd/Ca–O distances of the monocapped square antiprism polyhedron. See Table 1 for complementary information.

With the aim of studying in depth this anomalous behavior observed at low temperature, we have calculated the paramagnetic susceptibility of the Nd^{3+} below 140 K through the Simple Overlap Model (SOM) (19, 20). This model constitutes an alternative way for calculating the crystal field parameters from the atomic positions in the structure, as well as the angular overlap and the tree parameters models (21). It has been successfully applied to reproduce the phenomenological crystal field parameters for a great number of lanthanides as well as for some 3*d* elements and actinide compounds (22–25). SOM assumes that the crystal field effect can be calculated by considering a potential produced by an effective charge distribution over a small region, proportional to overlap integrals and situated around the mid-point of the metal–ligand distance. It calculates the B_q^k parameters by the relation

$$B_q^k = \langle r^k \rangle \sum_\mu g_\mu \rho_\mu e^2 \left(\frac{2}{1 \pm \rho_\mu}\right)^{k+1} \left(\frac{4\pi}{2k+1}\right)^{1/2} \frac{Y_q^{k*}(\Omega_\mu)}{R_\mu^{k+1}},$$

which is expressed as

$$B_q^k = \langle r^k \rangle \sum_\mu \rho_\mu \left(\frac{2}{1 \pm \rho_\mu}\right)^{k+1} A_q^k,$$

where A_q^k is the lattice sum of neighbors belonging to the first coordination sphere associated with a charge factor g_μ and to the usual spherical harmonics, $\langle r_q^k \rangle$ are the radial integrals whose numerical values are taken from (26) for the

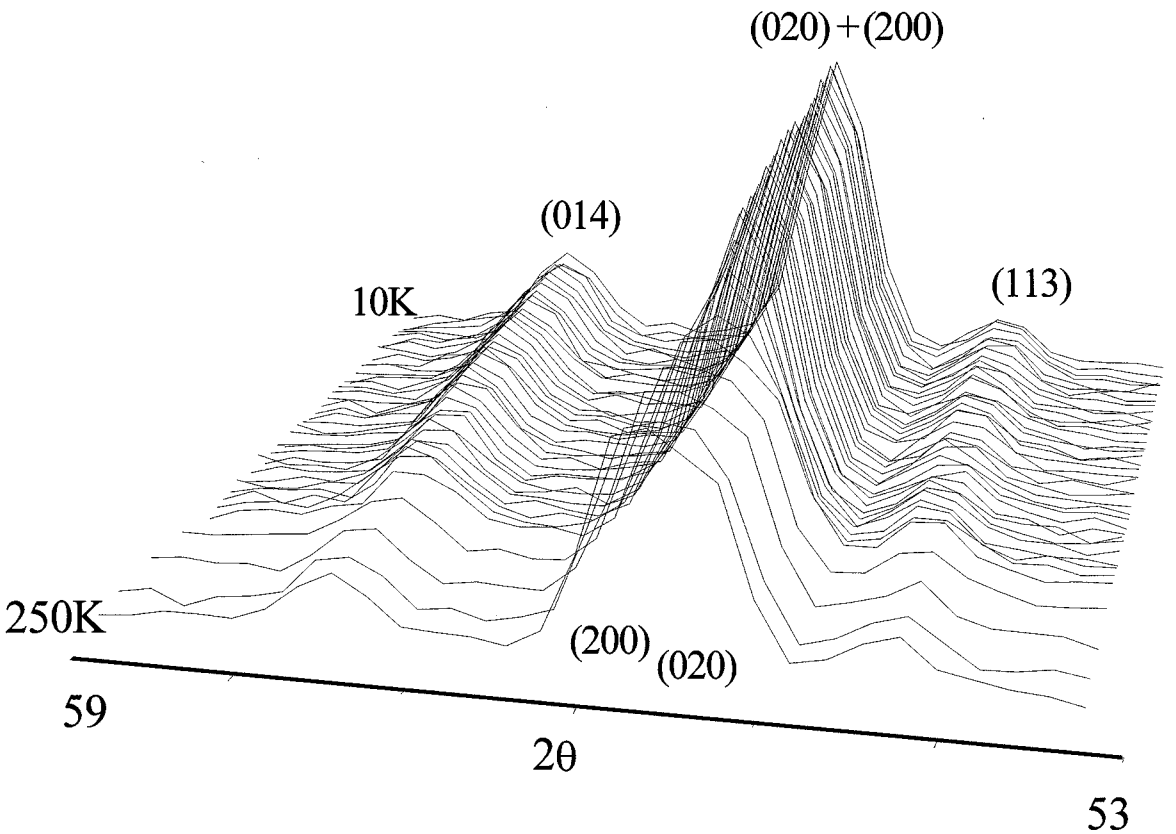

FIG. 4. Temperature dependence of the intensity of Bragg reflections ($53 < 2\theta < 59$) from neutron diffraction patterns obtained at low temperature ($T <$ RT).

rare earth ions, and ρ is the overlap between the $4f$ orbitals of the central ion and the s and p orbitals of each ligand. Its value varies as a function of the metal–ligand distance R, according to an exponential law $\rho = \rho_0(R_0/R)^{3.5}$ (27), R_0 being the shortest metal–ligand distance, the minus sign is applied when $r_{\text{metal}} < r_{\text{ligand}}$ (20, 28). The overlap value is small for the rare earths and for the actinides ($0.05 < \rho < 0.08$) (22). This is in agreement with the usually estimated values for the rare earths (29), for which the $4f$ orbitals are well protected from the chemical environment by external $5s$ and $5p$ closed subshells and take a small part in the chemical bonding. For the $3d$ elements the overlap is found within its expected range of values ($0.10 < \rho < 0.25$) (24).

The experimental susceptibility for $NdCaCrO_4$ and for Nd^{3+} calculated with SOM are displayed in Fig. 7, showing a very good agreement between 140 and 50 K. Here it is worth noting the lack of Cr^{3+} magnetic moment contribution to the susceptibility due to the antiferromagnetic order in the Cr^{3+} sublattices. Below 50 K a progressive disagreement between observed and calculated χ takes place and becomes very marked under 10 K. This behavior could indicate the appearance of short-range magnetic correlations of antiferromagnetic character within the Nd^{3+} sublattice, which justify on one hand the loss of the susceptibility signal observed experimentally and the deviation from the calculated χ, which does not take into account the possibility of magnetic interactions. On the other hand, due to the low dimensional nature of these magnetic correlations, they are compatible with the nonexistence of a long range magnetic order within the Nd^{3+} sublattices, as shown below based on neutron diffraction data. 3D magnetic ordering involving the Nd^{3+} is not favored by the chemical disorder (Ca^{2+}/Nd^{3+}) in the site $8f$.

Figure 8 shows a 3D-plot (intensity versus 2θ and temperature) of the obtained neutron diffraction patterns. The indexed reflections have been indicated together with their nuclear (n) or magnetic (m) reflection origin. Magnetic contribution to the nuclear scattered intensity is observed around 180 K. The gradual increase of the magnetic reflections below this temperature points to the existence of a progressive magnetic ordering. This behavior confirms the antiferromagnetic state in the Cr^{3+} sublattice proposed above from the magnetic susceptibility data. It is worth noting the notable coincidence between the Néel temperature for the Cr^{3+} sublattices and the sudden change in the slope of the thermal variation of lattice parameters shown in Fig. 5 which points to important magnetostriction effects in

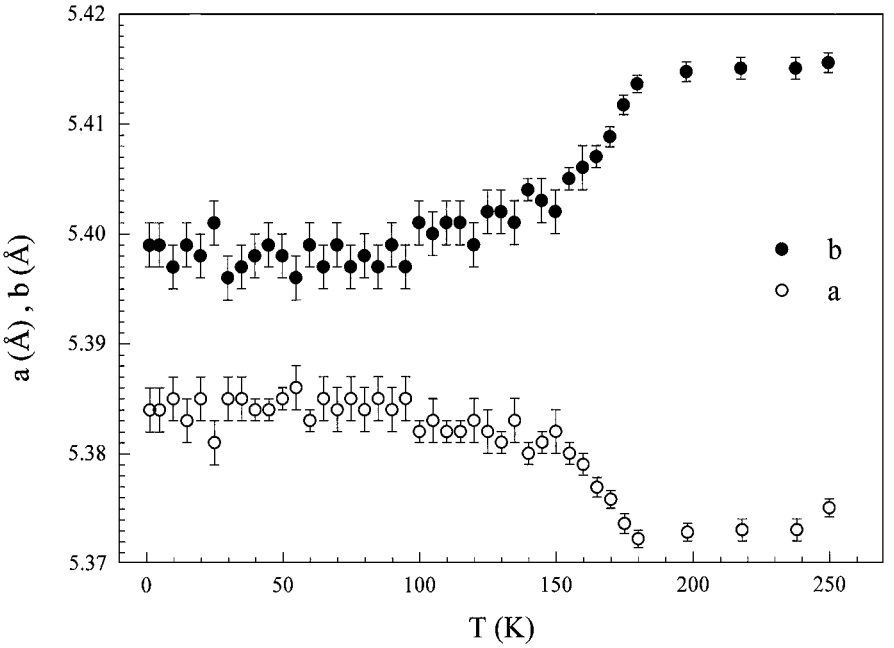

FIG. 5. Temperature dependence of the lattice parameters *a* and *b* below RT for $NdCaCrO_4$ oxide.

the structure. It is also worth noting the onset of the additional (100) magnetic reflection at 30 K, whose intensity increases progressively until 1.5 K (Fig. 8).

3.3. Magnetic Structure

All the magnetic reflections observed below 180 K have been indexed on the basis of a propagation vector $\mathbf{k} = [000]$. Numbering the four Cr magnetic sublattices in Wyckoff site 4*a* as 1 (0, 0, 0), 2 (1/2, 0, 1/2), 3 (0, 1/2, 1/2), and 4 (1/2, 1/2, 0); using the representation analysis, and taking as generators of *Bmab* space group the *B* centering translation *t* (1/2 0 1/2), the helical axis 2_{1y} and the rotation axis 2_z, one obtains the basis vectors for the irreducible representations of the space group *Bmab*, which could describe the magnetic order for the Cr^{3+} sublattices. The basis vectors are constructed from the linear combinations of the spin components of chromium atoms (30); see Table 2.

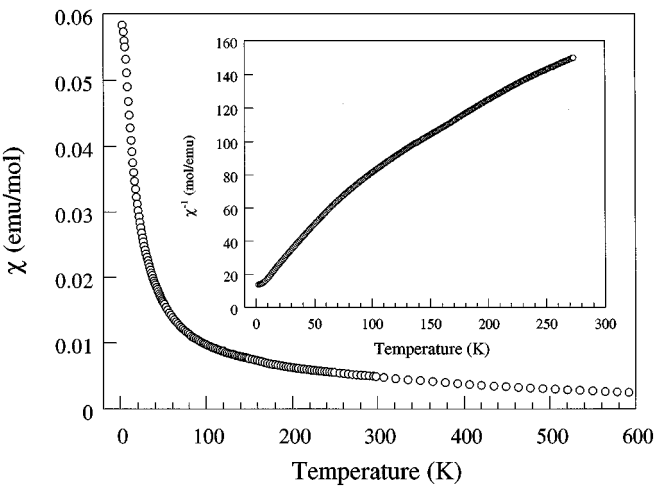

FIG. 6. Thermal dependence of the magnetic susceptibility for $NdCaCrO_4$ oxide. The inset shows the reciprocal susceptibility between 275 and 2 K.

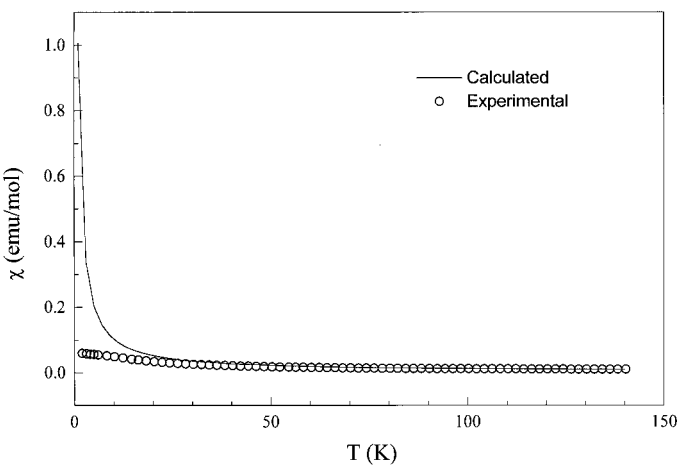

FIG. 7. Simulation of the paramagnetic susceptibility contribution of the Nd^{3+} ion in the $NdCaCrO_4$ oxide by the SOM method. Circles represent experimental data and the solid line the calculated data.

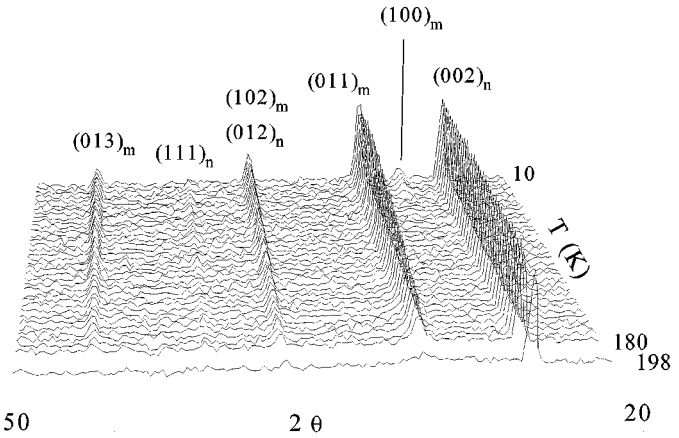

FIG. 8. Temperature evolution of the neutron diffraction patterns ($20 < 2\theta < 50$) obtained below RT for $NdCaCrO_4$ oxide.

Rietveld refinement of the powder diffraction data obtained between 180 and 35 K shows that the best fit, regarding the magnetic reflections, is obtained with either G_x or C_yF_z, with $F_z = 0$, magnetic modes. The (011), or (101), magnetic reflection is the most intense one for these modes; see Fig. 8. However, it is rather difficult to distinguish between both magnetic modes due to the pseudotetragonal symmetry of the crystal structure in that temperature range. Figure 9a shows the neutron diffraction pattern obtained at 100 K refined considering the G_x mode. Therefore, the $NdCaCrO_4$ oxide from 180 to 35 K presents the Cr^{3+} magnetic moments antiferromagnetically ordered in the xy plane, along either $x(G_x)$ or $y(C_y)$ directions; see Fig. 10a. The Cr^{3+} magnetic moment value obtained at 35 K is 2.5(1) μ_B. This collinear magnetic structure is the same as

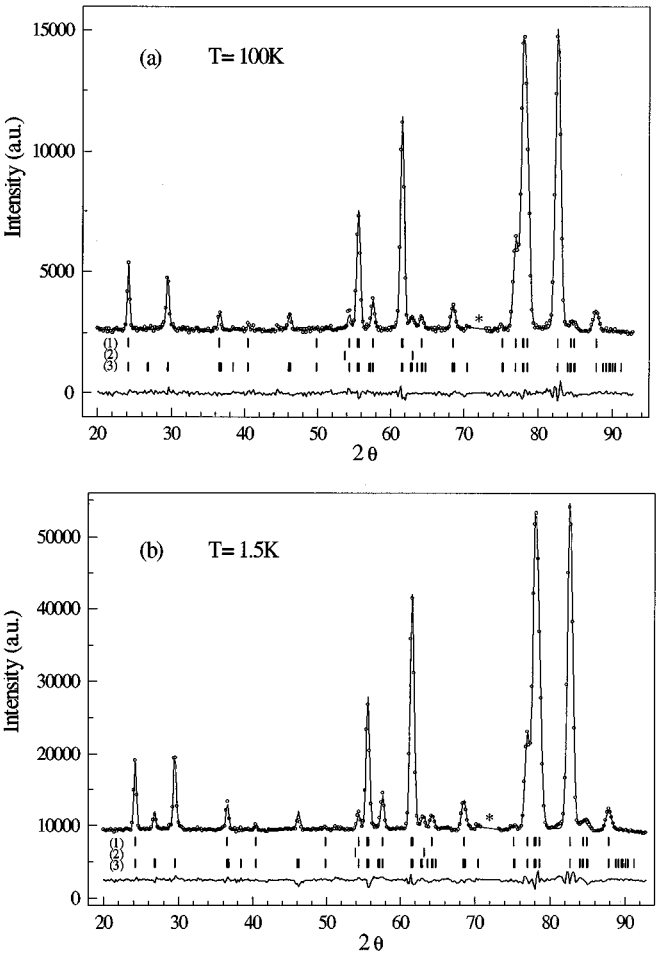

FIG. 9. Neutron powder diffraction patterns (D1B) obtained at (a) 100 and (b) 1.5 K. Circles represent raw data and the solid line is the calculated profile. Rows (1)and (2) are the position of the allowed structural Bragg reflections for $NdCaCrO_4$ and CaO oxides, respectively; row (3) corresponds to the magnetic ones for $NdCaCrO_4$ oxide. A difference curve is plotted at the bottom of the pattern. Reliability factors: (a) $R_{wp} = 6.69\%$, $R_B = 1.68\%$, $\chi^2 = 1.84$, and $R_M = 13.5\%$; (b) $R_{wp} = 5.51\%$, $R_B = 2.26\%$, $\chi^2 = 4.89$, and $R_M = 10.7\%$. The asterisks indicate a small excluded area due to the sample environment.

TABLE 2

Basis Vectors for the Irreducible Representations of Cr Sublattices in *Bmab* (k = 0), and Rules for Allowed Magnetic Reflections

	x	y	z
$\Gamma_1(+++)$	C	—	—
$\Gamma_2(++-)$	—	F	C
$\Gamma_3(+-+)$	—	C	F
$\Gamma_4(-++)$	—	G	A
$\Gamma_5(+--)$	F	—	—
$\Gamma_6(-+-)$	A	—	—
$\Gamma_7(--+)$	G	—	—
$\Gamma_8(---)$	—	A	G

$F = S_1 + S_2 + S_3 + S_4$; $h + l$, $k + l$, $h + k$. All even.
$G = S_1 - S_2 + S_3 - S_4$; $h + l$ = odd, $k + l$ = even, $h + k$ = odd.
$C = S_1 + S_2 - S_3 - S_4$; $h + l$ = even, $k + l$ = odd, $h + k$ = odd.
$A = S_1 - S_2 - S_3 + S_4$; $h + l$ = odd, $k + l$ = odd, $h + k$ = even.

Note. S_i represents a spin component of atom in i sublattice of the 4a site.

that proposed for the isostructural $PrCaCrO_4$ oxide (15). However, while in the praseodymium phase this magnetic structure remains until 1.5 K, in the case of the neodymium phase the onset of the mentioned extra magnetic reflection (100), or (010), at 30 K (see Fig. 8) is indicative of certain changes in the magnetic structure. The appearance of this reflection growing from 30 to 1.5 K is due to a spin reorientation in the Cr^{3+} sublattices, which not only involves a change in the magnetic moment direction but a change in the coupling of the Fourier components. So it is possible to consider it as a magnetic phase transition from the magnetic structure shown in Fig. 10a to that in Fig. 10b, which means the gradual appearance of an antiferromagnetic ordered component along the z direction.

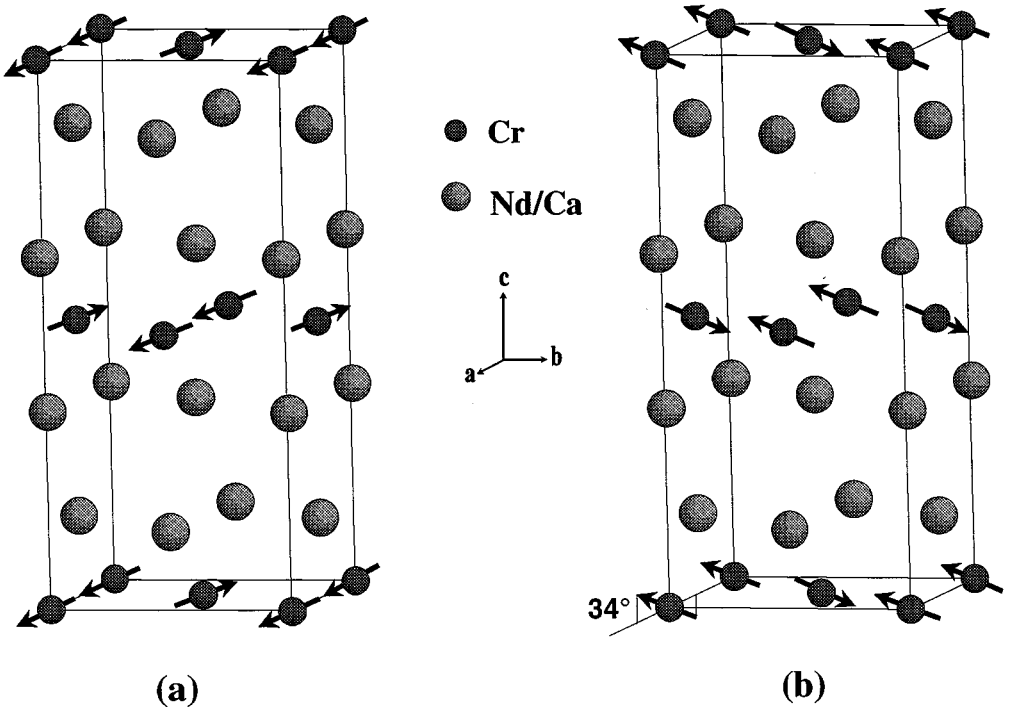

FIG. 10. Proposed magnetic structures for $NdCaCrO_4$ oxide, (a) between 180 and 35 K (G_x mode) and (b) below 30 K until1.5 K (G_x and F_yC_z modes with $F_y = 0$).

The fit of the diffraction patterns corresponding to this temperature range is only fulfilled considering the mixing of irreducible representations, whose first consequence is that the magnetic structure no longer remains collinear. The best fit is obtained with a model $\Gamma_7 \oplus \Gamma_2$ involving the basis vectors G_x and F_yC_z, with $F_y = 0$ (see Fig. 9b) and the magnetic moments held in the xz plane (see Fig. 10b). A non-null F_y mode with $\mathbf{k} = 0$ means a net ferromagnetic component in the y direction that is not observed in the magnetic measurements and neutron data. Another possibility to fit the pattern is by mixing Γ_3 (C_yF_z) and Γ_8 (A_yG_z) with $A_y = F_z = 0$ and therefore the magnetic moment on the yz plane. This rather strange combination considering the orthogonality conditions for basis functions removes in turn certain ambiguity in the possible modes considered before for $PrCaCrO_4$ and $NdCaCrO_4$ over 30 K; it seems more reasonable $\Gamma_7(G_x)$ than Γ_3 (C_y, $F_z = 0$). The obtained magnetic moment at 1.5 K from the Rietveld refinement shown in Fig. 9b is $\mu = 2.73(9)\ \mu_B$ near the expected value $2S = 3\ \mu_B$; the components are $\mu_x = 2.25(9)\ \mu_B$ and $\mu_z = 1.5(1)\ \mu_B$.

On the other hand, there is no indication of contribution on magnetic Bragg reflections coming from the rare earths, and it is not surprising that the Nd^{3+} ions remains magnetically disordered until 1.5 K, because they are magnetically diluted by the presence of the diamagnetic Ca^{2+} ions randomly distributed within the same crystallographic position. Nevertheless, the temperature at which the spin reorientation takes place, 30 K, coincides with the temperature at which the experimental magnetic susceptibility values start to be noticeably different from the calculated ones; see Fig. 7. This fact seems to indicate that the spin reorientation of the Cr^{3+} sublattices could be induced by the onset of local magnetic interactions between Nd^{3+} and Cr^{3+} ions. This interpretation could justify the absence of a spin reorientation in the magnetic structure of the isomorphous $PrCaCrO_4$ oxide, since it has been proposed that the temperature-independent paramagnetism observed below 20 K in this oxide is owing to the existence of a non-magnetic ground state of the Pr^{3+} ion (31). On the other hand, the magnetostriction effects clearly marked in this system could indicate the coupling of order parameters of lattice distortions and magnetic nature, and so the anisotropic terms in the spin Hamiltonian are rather important and may justify the admixture of different modes (30).

Some additional work is now in progress in the isostructural $RCaCrO_4$ (R = Sm, Eu) in order to establish the influence of the nature of the ground crystal field term of the R^{3+} ion in the magnetic behavior of this family of $RCaCrO_4$ compounds.

ACKNOWLEDGMENTS

The authors thank the Comisión Interministerial de Ciencia y Tecnología for financial support under Project MAT97-0697.

REFERENCES

1. G. Wagner and D. Balz, *Z. Elektrochem.* **56,** 574 (1952).
2. J. G. Bednorz and A. K. Müller, *Z. Phys. B* **64,** 189 (1986).
3. J. Rodríguez-Carvajal, J. L. Martínez, J. Pannetier, and R. Sáez-Puche, *Phys. Rev. B* **38,** 7148 (1988).
4. I. D. Brown, *Z. Kristallogr.* **199,** 255 (1992).
5. R. Sáez Puche, F. Fernández, J. Rodríguez Carvajal, and J. L. Martínez, *Solid State Commun.* **72,** 273 (1989).
6. J. Rodríguez-Carvajal, M. T. Fernández-Díaz, and J. L. Martínez, *J. Phys. Condens. Matt.* **3,** 3215 (1991).
7. G. H. Lander, P. J. Brown, J. M. Honig, and J. Spálek, *Phys. Rev. B* **40,** 4463 (1989).
8. J. Rodríguez-Carvajal, M. T. Fernández-Díaz, J. L. Martínez, F. Fernández, and R. Sáez-Puche, *Europhys. Lett.* **11**(3), 261 (1990).
9. M. T. Fernández-Díaz, J. Rodríguez-Carvajal, J. L. Martínez, G. Fillion, F. Fernández, and R. Sáez-Puche, *Z. Phys. B Condens. Matt.* **82,** 275 (1991).
10. X. Obradors, X. Batlle, J. Rodríguez-Carvajal, J. L. Martínez, M. Vallet, J. M. González-Calbet, and J. Alonso, *Phys. Rev. B* **43,** 10451 (1991).
11. A. Daoudi and G. Le Flem, *Mater. Res. Bull.* **8,** 1103 (1973).
12. R. Berjoan, J. P. Coutures, G. Le Flem, and M. Saux, *J. Solid State Chem.* **42,** 75 (1982).
13. J. Romero, R. Sáez Puche, F. Fernández, J. L. Martínez, Q. Chen, M. Castro, and R. Burriel, *J. Alloys Comp.* **225,** 203 (1995).
14. J. L. Martínez, M. T. Fernández-Díaz, Q. Chen, C. Prieto, A. de Andrés, R. Sáez-Puche, and J. Romero, *J. Mag. Mag. Mater.* **140,** 1179 (1995).
15. J. Romero de Paz, M. T. Fernández-Díaz, J. Hernández Velasco, R. Sáez Puche, and J. L. Martínez, *J. Solid State Chem.* **142,** 29 (1999).
16. "Guide to Neutron Research Facilities at the ILL". Institut Max von Laue-Paul Langevin. Grenoble, France, 1988.
17. R. A. Young, Ed., "The Rietveld Method." IUCr, Oxford Science, New York, 1995.
18. J. Rodríguez-Carvajal, *in* "Abstracts of Satellite Meeting on Powder Diffraction of the XV Congress of the International Union of Crystallography," Toulouse, 1990.
19. O. L. Malta, *Chem. Phys. Lett.* **87,** 27 (1982).
20. O. L. Malta, *Chem. Phys. Lett.* **88,** 353 (1982).
21. P. Porcher, *in* "Rare Earths" (R. Sáez and P. A. Caro, Eds.), p. 43. Editorial Complutense, Madrid, 1998.
22. O. L. Malta and G. F. De Sá, *Quim. Nova* (*Brazil*) **6,** 123 (1983).
23. O. L. Malta, S. L. J. Ribeiro, M. Faucher, and P. Porcher, *J. Phys. Chem. Solids* **52,** 587 (1991).
24. J. Derouet, L. Beaury, P. Porcher, R. Olazcuaga, J. M. Dance, G. Le Flem, M. El Bouari, and A. El Jazouli, *J. Solid State Chem.* **143,** 230 (1999).
25. P. Porcher, M. Couto Dos Santos, and O .L. Malta, *Phys. Chem. Chem. Phys.* **1,** 397 (1999).
26. A. J. Freeman and P. J. Desclaux, *J. Mag. Mag. Mater.* **12,** 11 (1979).
27. C. K. Jørgensen, "Modern Aspects of Ligand Field Theory." North-Holland, Amsterdam, 1971.
28. G. P. Barnett, M. C. Pires Costa, and R. Ferreira, *Chem. Phys. Lett.* **25,** 49 (1974).
29. G. Burns, *J. Chem. Phys.* **42,** 377 (1965).
30. E. F. Bertaut, *in* "Magnetism" (G. T. Rado and H. Suhl, Eds.), Vol. III, p. 149. Academic Press, New York, 1963.
31. J. Romero, Ph.D. Thesis, Universidad Complutense de Madrid, 1998.